A Nonlinear-Model-Based Observer for a State-of-Charge Estimation of a Lithium-ion Battery in Electric Vehicles

Woo-Yong Kim [1] , Pyeong-Yeon Lee [2], Jonghoon Kim [2],* and Kyung-Soo Kim [1],*

[1]   Department of Mechanical Engineering, Korea Advanced Institute of Science and Technology, Daejeon 291, Korea
[2]   Department of Electric Engineering, Chungnam National University, Daejeon 99, Korea
*   Correspondence: whdgns0422@cnu.ac.kr (J.K.); kyungsookim@kaist.ac.kr (K.-S.K.)

check for updates

Abstract: This paper presents a nonlinear-model-based observer for the state of charge estimation of a lithium-ion battery cell that always exhibits a nonlinear relationship between the state of charge and the open-circuit voltage. The proposed nonlinear model for the battery cell and its observer can estimate the state of charge without the linearization technique commonly adopted by previous studies. The proposed method has the following advantages: (1) The observability condition of the proposed nonlinear-model-based observer is derived regardless of the shape of the open circuit voltage curve, and (2) because the terminal voltage is contained in the state vector, the proposed model and its observer are insensitive to sensor noise. A series of experiments using an INR 18650 25R battery cell are performed, and it is shown that the proposed method produces convincing results for the state of charge estimation compared to conventional SOC estimation methods.

Keywords: nonlinear battery model; state of charge estimation; lithium-ion battery; Lipschitz nonlinear system; Luenberger observer

1. Introduction

Since the first development of hybrid electrical vehicles (HEVs), pure electric vehicles (EVs) have been rapidly commercialized. In contrast to HEVs, the mileage range of EVs is directly affected by the power and energy density of the battery itself and the performance of the battery management system (BMS). Hence, many studies related to lithium-ion (Li-ion) batteries, including the development of new materials and algorithms for inner state estimation, have been conducted by various research groups [1–8]. Increasing the energy and power density via advancements in battery manufacturing technology requires a higher level of monitoring of the battery states to fully and safely use the potential of the battery.

In EV applications, the state of charge (SOC), which represents the amount of charge in the battery, is the most important parameter because it directly relates to the number of miles that an EV can travel. An inaccurate SOC information causes the driver to constantly worried about the EV stopping on the road or the battery being overcharged/overdischarged, causing ignition or explosion. Therefore, it is important to estimate the SOC and accurately determine the dischargeable capacity of the battery to protect the battery itself and help reduce the driver's anxiety [9–11]. However, unlike the voltage and current, there is no way to measure the SOC directly. Hence, advanced algorithms for accurate SOC estimation need to be researched.

Typically, there are two kinds of categories of SOC estimation methods: (1) model-less and (2) model-based methods. The most famous example of a model-less algorithm is the Coulomb

counting method [12,13]. This method estimates the SOC by integrating the current through the battery. Its simplicity and low computational cost make this method valuable in the infancy of the BMS. However, it has obvious limitations: it suffers from an initial condition problem and the accumulation of sensor offset due to the integrator. Artificial neural networks (ANNs) and fuzzy algorithms are also model-less methods that implement intelligent algorithms [14–16]. However, these data-driven methods have inherent problems, such as a long training time and a large number of data sets. In particular, when the type of battery cell is changed, the learning procedure has to be restarted. This is far from a practical concept. On the other hand, model-based methods use an equivalent electrochemical model (EECM) or electrical circuit model (ECM) to represent the current-voltage relationship of the battery. The EECM formulates the key behaviors of the battery cell by deriving a series of differential equations for the chemical reactions inside the battery cell [17,18]. The accuracy of the EECM for SOC estimation is very high, but its practical usefulness is questionable, because a very high complexity leads to a significant memory and computational burden. On the other hand, the ECM represents the current-voltage relationship by using electric components such as resistance, capacitance and a variable voltage source [19–22]. Although the ECM is relatively inaccurate compared with the EECM, the ECM is commonly adopted for real-time SOC estimation because it can be simply implemented and can achieve a high accuracy when the ECM cooperates with a state observer. Therefore, there have been many studies on various state observers and various kinds of ECMs.

The Kalman-filter-based observer, Luenberger observer, sliding-mode observer and proportional-integral observer are widely used for the SOC estimation [23–35]. Previous studies have verified that all methods produce good performance for the online SOC estimation. However, while the battery is a type of nonlinear system due to the nonlinear relationship between the SOC and open circuit voltage (OCV), previous studies focused on linear systems and their observers. Therefore, linearization techniques must be implemented. For example, Kalman-filter-based approaches apply a Taylor series expansion to each operating point at each time step, and the other approaches apply the 'piece-wise' linearization technique, which divides the nonlinear function into multiple linear functions according to each operating region. Linearization techniques are useful for approximating a nonlinear system, but when the operating point changes, the model of the linearized system changes. This means that the performance of the designed observer based on a linearized model at a certain operating point changes with respect to the operating region, and even worse, there can be a critical point where the observer loses its stability. However, most previous studies did not consider time-varying conditions.

This paper proposes a nonlinear model for a battery cell and a nonlinear-model-based observer. This work has two contributions. First, this paper proposes a nonlinear state space representation of a 1st-order Thevenin equivalent circuit model. This allows the system to be time-invariant and the eigenvalues of the designed observer to be fixed in all operating regions. The resulting observability condition of the proposed model, which is generally used as the necessary condition for the design of an observer, is derived regardless of the shape of the open-circuit voltage curve. This means that the observability condition is always satisfied even if there is a voltage plateau on the open-circuit voltage curve [36–38]. The proposed nonlinear model is also insensitive to sensor noise, because the state vector contains the terminal voltage. Second, a nonlinear-model-based Luenberger observer that can address the nonlinear system model is proposed. The stability condition of the proposed observer is strictly derived using nonlinear system theories. The performance of the real-time SOC estimation of the proposed method is evaluated by conducting experiments with INR 18650 25R from SAMSUNG SDI.

2. Nonlinear System Model for a Single Battery Cell

There are many ECMs for battery cells. For an onboard BMS system, there is always a trade-off between the model accuracy and complexity. Therefore, a suitable selection for the ECM must be made according to the application. Generally, for real-time SOC estimation, the 1st-order Thevenin ECM [5] is adopted because it is more suitable for real-time SOC estimation (see Figure 1).
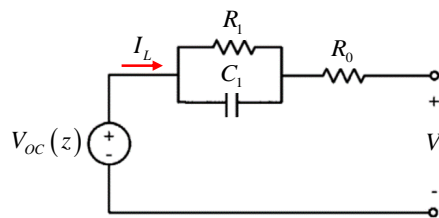
Figure 1. Thevenin's equivalent circuit model with a single RC pair.

The dynamic equations of the selected ECM are derived as follows:

$$V_t = V_{OC}(z) - I_L R_0 - V_1, \tag{1}$$

$$\dot{z} = -\frac{I_L}{C_n}, \tag{2}$$

$$\dot{V_1} = -\frac{1}{C_1 R_1} V_1 + \frac{1}{C_1} I_L \tag{3}$$

where V_t is the terminal voltage of the battery cell, $V_{OC}(z)$ is the OCV function of z, z represents the SOC, I_L is the load current, R_0 is the equivalent internal resistance, V_1 is the voltage of the RC pair, C_n is the nominal capacity, R_1 is the equivalent resistance of the RC pair and C_1 is the equivalent capacitance of the RC pair. In the case of a Li-ion battery, the nonlinear function $V_{OC}(z)$ representing the relationship between the SOC and OCV always exists. This makes it difficult to build a state space model and design a state observer for the battery system.

2.1. Linearized System Model for a Single Battery Cell

Most previous studies related to observer-based SOC estimation [29,30,32,34,39] linearized $V_{OC}(z)$ by using a piece-wise assumption. The linearized $V_{OC}(z)$ is defined as

$$V_{OC}(z) = k_i z + d_i, \quad for \ the \ i^{th} \ SOC \ region \tag{4}$$

where k_i and d_i are the coefficients of each linearized $V_{OC}(z)$ and i is the number of divided sections of the SOC. (1)–(3) can be rewritten as a linear state space representation by using (4).

$$\begin{aligned} \dot{x} &= Ax + Bu, \\ y_i &= C_i x + Du \end{aligned} \tag{5}$$

where $x = \begin{bmatrix} V_1 & z \end{bmatrix}^T$, $y_i = V_t - d_i$, $A = \begin{bmatrix} -\frac{1}{C_1 R_1} & 0 \\ 0 & 0 \end{bmatrix}$, $B = \begin{bmatrix} \frac{1}{C_1} & -\frac{1}{C_n} \end{bmatrix}^T$, $u = I_L$, $C_i = \begin{bmatrix} -1 & k_i \end{bmatrix}$ and $D = R_0$. By utilizing this linearized system model for a single battery cell, it is easy to implement the state observer for an SOC estimation because the theories for linear systems are applicable. However, a major concern of this linearized model is that when the operating point changes, the linearized system model will change. If the change is large, the optimally designed observer will no longer be optimal, and in the worst case, the observer will become unstable. Details about the limitations of the linearized model for the battery system are mentioned in the discussion section.

2.2. Nonlinear System Model for a Single Battery Cell

This paper proposes a nonlinear state space representation for the battery cell. Let us define the nonlinear function $V_{OC}(z)$ as a summation of a linear term and a nonlinear term as

$$V_{OC}(z) = \alpha z + \beta + f(z),$$
$$f(z) = \sum_{n=1}^{N} a_n \sin(b_n z + c_n) \tag{6}$$

where α and β are the coefficients of the linear term, $f(z)$ is a bounded nonlinear function consisting of a sum of sine functions and a_n, b_n, and c_n are the coefficients of the sum of sine functions. Figure 2 conceptually represents (6).
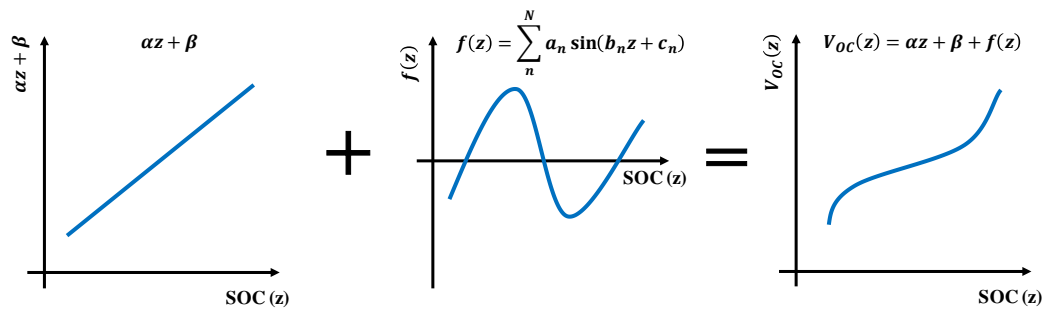

Figure 2. Reformulation of the open-circuit voltage representation.

Equations (1)–(3) can be rewritten as a nonlinear state space representation by using (6). The terminal voltage of the ECM in (1) is

$$V_t = \alpha z + \beta + f(z) - V_1 - I_L R_0. \tag{7}$$

Its time derivative can be calculated as follows:

$$
\begin{aligned}
\dot{V}_t &= \alpha \dot{z} + \frac{d}{dt}f(z) - \dot{V}_1 - \dot{I}_L R_0 = -\alpha \frac{1}{C_n} I_L + \frac{d}{dz}f(z)\dot{z} - \left(-\frac{1}{C_1 R_1}V_1 + \frac{1}{C_1}I_L\right) \\
&= -\alpha \frac{1}{C_n} I_L - \frac{d}{dz}f(z)\frac{1}{C_n}I_L + \frac{1}{C_1 R_1}V_1 - \frac{1}{C_1 R_0}(\alpha z + \beta + f(z) - V_1 - V_t) \\
&= \frac{1}{C_1 R_0}V_t + \left(\frac{1}{C_1 R_1} + \frac{1}{C_n R_0}\right)V_1 - \frac{\alpha}{C_1 R_0}z + \left\{-\frac{1}{C_n}I_L\frac{d}{dz}f(z) - \frac{1}{C_1 R_0}f(z)\right\} + \left\{-\frac{\alpha}{C_n}I_L - \frac{\beta}{C_1 R_0}\right\}.
\end{aligned} \tag{8}
$$

The derivative of the state of charge in (2) is

$$
\begin{aligned}
\dot{z} &= -\frac{1}{C_n R_0}(\alpha z + \beta + f(z) - V_1 - V_t) \\
&= \frac{1}{C_n R_0}V_t + \frac{1}{C_n R_0}V_1 - \frac{\alpha}{C_n R_0}z - \frac{1}{C_n R_0}f(z) - \frac{1}{C_n R_0}\beta.
\end{aligned} \tag{9}
$$

Then, the nonlinear state space representation of the given ECM can be obtained as

$$\dot{x} = Ax + F(x, I_L) + G(I_L),$$
$$y = Cx,$$

$$A = \begin{bmatrix} \frac{1}{R_0 C_1} & \frac{1}{R_0 C_1} + \frac{1}{R_1 C_1} & -\frac{\alpha}{R_0 C_1} \\ 0 & -\frac{1}{R_1 C_1} & 0 \\ \frac{1}{R_0 C_n} & \frac{1}{R_0 C_n} & -\frac{\alpha}{R_0 C_n} \end{bmatrix}, \quad F(x, I_L) = \begin{bmatrix} -\frac{1}{R_0 C_1}f(z) - \frac{1}{C_n}\frac{d}{dz}f(z)I_L \\ 0 \\ -\frac{1}{R_0 C_n}f(z) \end{bmatrix},$$

$$G(I_L) = \begin{bmatrix} -\frac{1}{C_n}\alpha I_L - \frac{1}{R_0 C_1}\beta \\ \frac{I_L}{C_1} \\ -\frac{1}{R_0 C_n}\beta \end{bmatrix}, \quad x = \begin{bmatrix} V_t \\ V_1 \\ z \end{bmatrix}, \quad y = V_t \tag{10}$$

where A is the state matrix, $F(z, I_L)$ is a nonlinear function with unknown states and $G(I_L)$ is a nonlinear function with known parameters. It is noted that the time derivative of the current I_L can be negligible not only because the sampling time of the algorithm is much faster than the current change [30] but also because its effect is much smaller than that of the other factors. Different from the linearized model in (5), it is easily shown that the proposed nonlinear system model in (10) does not change regardless of the SOC range, and the state vector contains the terminal voltage V_t, which can lead to the model being insensitive to sensor noise when using the measured value directly. However, because of the existence of the nonlinear functions $F(z, I_L)$ and $G(I_L)$, the observers used previously for linear systems are no longer available, and the stability condition for the nonlinear-model-based observer is not determined by considering the eigenvalues of the linear stability matrix $(A - LC)$, where L is the observer gain matrix. Hence, in the next section, a nonlinear-model-based observer is proposed, and its stability condition is verified based on the Lyapunov stability criteria.

3. Nonlinear-Model-Based Observer Design

Theorem 1. *Under the assumptions that the linear observability matrix $(A - L_nC)$ of the given nonlinear system model in (10) has full rank, and the nonlinear function $F(z, I_L)$ can be assumed to be a locally Lipschitz continuous function with a Lipschitz constant χ, which satisfies (11) in the physically feasible range of space X such that*

$$\|F(x_1, I_L) - F(x_2, I_L)\| \leq \chi \|x_1 - x_2\|, \forall x \in X, \tag{11}$$

the observer given in (12) is asymptotically stable if the Luenberger observer gain L_n can be chosen to ensure that the linear stability matrix $(A - L_nC)$ is Hurwitz and the inequality (13) is satisfied.

$$\dot{\hat{x}} = A\hat{x} + F(\hat{x}, I_L) + G(I_L) + L_n(y - C\hat{x}), \tag{12}$$

$$\min_{\omega \in R^+} \sigma_{\min}(A - L_nC - j\omega I) > \chi \tag{13}$$

where χ is the Lipschitz constant in (11).

Proof. Let us prove Theorem 1 by the method of contradiction. According to H_∞ theory, the following well-known condition is satisfied. If the Hamiltonian matrix

$$H = \begin{bmatrix} A & R \\ Q & -A^T \end{bmatrix} \tag{14}$$

has no imaginary eigenvalues; then, there exists a symmetric matrix P satisfying the algebraic Riccati equation

$$A^TP + PA + PRP - Q = 0 \tag{15}$$

(for a proof, see [40]). In the same context, it can said if that the Hamiltonian matrix

$$H = \begin{bmatrix} (A - L_nC) & \chi^2 I \\ -I - \varepsilon I & -(A - L_nC)^T \end{bmatrix} \tag{16}$$

has no imaginary eigenvalues, there exists a symmetric matrix P satisfying the algebraic Riccati equation

$$(A - L_nC)^TP + P(A - L_nC) + P\chi^2P + I + \varepsilon I = 0. \tag{17}$$

From (13), there exists a finite ω_0 such that

$$\min_{\omega \in R^+} \sigma_{\min}(A - L_nC - j\omega I) > \sigma_{\min}(A - L_nC - j\omega_0 I) = \chi_{\min}. \tag{18}$$

Then, we can say that for all $\omega > \omega_0$, $(A - L_n C - j\omega I)^* (A - L_n C - j\omega I) \geq \chi_{\min}^2 I$ is satisfied, where * indicates a Hermitian matrix. Choose ϵ such that

$$(A - L_n C - j\omega I)^* (A - L_n C - j\omega I) \geq \chi_{\min}^2 I > \chi^2 (I + \varepsilon I). \tag{19}$$

The eigenvalues of the Hamiltonian matrix (16) are given by [41]

$$\det \left[\chi^2 (I + \varepsilon I) + \{\lambda I + (A - L_n C)^T\}\{\lambda I + (A - L_n C)\} \right] = 0. \tag{20}$$

Without loss of generality, it can assumed that an imaginary axis eigenvalue is represented by $j\omega$. By substituting $\lambda = j\omega$ in (20), we have

$$\det \left[\chi^2 (I + \varepsilon I) + \{-j\omega I + (A - L_n C)^T\}\{-j\omega + (A - L_n C)\} \right] = 0. \tag{21}$$

This means that

$$\{(A - L_n C)^T - j\omega I\}\{(A - L_n C) - j\omega\} = \chi^2 (I + \varepsilon I). \tag{22}$$

This contradicts (19). Hence, the matrix H in (16) cannot have any imaginary eigenvalues if inequality in (13) satisfied.

Let us define the state estimation error vector as $e = x - \hat{x}$ and consider the Lyapunov function candidate $V = e^T P e$. Then, the derivative of V is

$$\begin{aligned}
\dot{V} &= \dot{e}^T P e + e^T P \dot{e} \\
&= e^T \left[(A - L_n C)^T P + P (A - L_n C) \right] e + 2 e^T P \left[F(x, I) - F(\hat{x}, I) \right].
\end{aligned} \tag{23}$$

Using the Lipschitz condition in (11) and the property $e^T P \left[F(x, I) - F(\hat{x}, I) \right] \leq \|P e\| \, \|F(x, I) - F(\hat{x}, I)\|$, the derivative of V can be represented by an inequality as

$$\dot{V} < e^T \left[(A - L_n C)^T P + P (A - L_n C) \right] e + 2\chi \, \|P e\| \, \|e\|. \tag{24}$$

Using

$$\chi^2 e^T P P e + e^T e = 2\chi e^T P e \geq 2\chi \, \|P e\| \, \|e\|, \tag{25}$$

and the result of (16)–(22), the upper bound of the Lyapunov candidate can be obtained as

$$\dot{V} \leq e^T \left[(A - L_n C)^T P + P (A - L_n C) + \chi^2 P P + I \right] e = -e^T \varepsilon I e. \tag{26}$$

Hence, the system is asymptotically stable. □

There are two kinds of necessary conditions for Theorem 1: (1) the linear observability matrix $(A - L_n C)$ of a given system has full rank, and (2) the nonlinear function is a local Lipschitz continuous function. The linear observability matrix of the given nonlinear system model in (10) can be obtained as $O_{(A,C)} = \begin{bmatrix} C & CA & CA^2 \end{bmatrix}^T$.

The linear observability matrix of the given system is derived as

$$O_{(A,C)} = \begin{bmatrix} 1 & 0 & 0 \\ p_1 & p_1 + p_2 & -\alpha p_1 \\ p_1^2 - \alpha p_1 p_3 & p_1^2 - p_2^2 - \alpha p_1 p_3 & -\alpha p_1^2 + \alpha^2 p_1 p_3 \end{bmatrix} \tag{27}$$

where $p_1 = \frac{1}{R_0 C_1}$, $p_2 = \frac{1}{R_1 C_1}$ and $p_3 = \frac{1}{R_0 C_n}$. The determinant of the matrix $O_{A,C}$ is

$$\det \left| O_{(A,C)} \right| = \alpha p_3 - p_1 - p_2. \tag{28}$$

It is shown that the given observability condition is independent of the shape of the OCV function. This is a function of the given parameters. Then, if the coefficient α is selected such that

$$\alpha \neq \frac{p_1 + p_2}{p_3}, \tag{29}$$

the given nonlinear battery model in (10) will satisfy the first necessary condition of Theorem 1. The Lipschitz condition in (11) can be rewritten by the following partial differential equation [42] as

$$\frac{|F(x_1, I_L) - F(x_2, I_L)|}{|x_1 - x_2|} = \left. \frac{\partial F(x, I_L)}{\partial x} \right|_{\forall x \in X} \leq \chi. \tag{30}$$

While there are three kinds of states to be considered for the Lipschitz condition, the state V_t is measurable. Therefore, the two unmeasurable states, V_1 and z, must be considered. The Lipschitz conditions for the nonlinearities of V_1 and z can be derived as follows:

$$\frac{\partial F_2(x, I_L)}{\partial x} = 0, \tag{31}$$

$$\frac{\partial F_3(x, I_L)}{\partial x} = -\frac{1}{R_0 C_n} \frac{d}{dz} f(z) \tag{32}$$

where F_2 and F_3 are the nonlinearities of V_d and z. As mentioned above, the function $f(z)$ is predefined by the sum of the sinusoidal function, which has a certain boundary. The resulting function in (32) is a function of only one state value z. Therefore, if the function values of (32) in the overall feasible range of z are smaller than the Lipschitz constant χ, the inequality in (11) is satisfied. This means that the second necessary condition of the Theorem 1 is satisfied. The specific parameters of the necessary conditions will be verified in the next section.
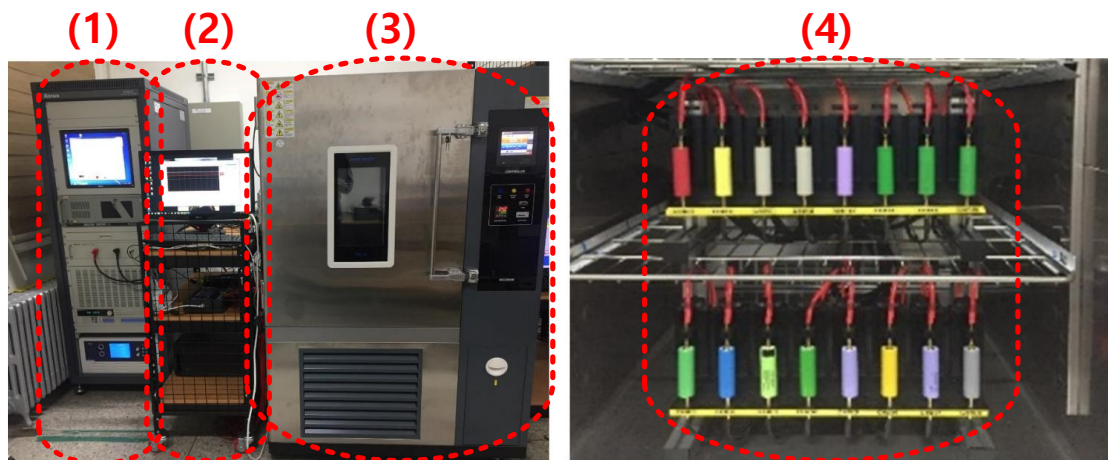
4. Experiments

This section inspects the performance of the SOC estimation of the proposed nonlinear battery model and the extended Kalman filter, which has commonly been applied for SOC estimation in previous works in [11,24,38,43] by conducting a series of experiments.
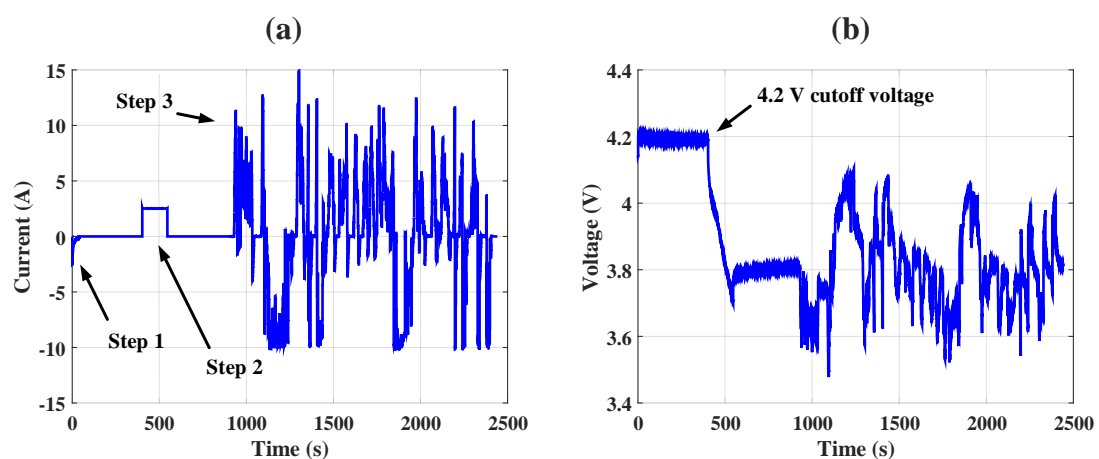
4.1. Experimental Setup

To analyze the performance of the SOC estimation of the proposed observer and previous methods, an experimental battery cell test bench is established. Experiments were conducted using the INR 18650-25R battery cell from SAMSUNG SDI. The test bench for the charge-discharge experiment is shown in Figure 3. The setup consists of a bidirectional DC/DC converter (Maccor 4300 K), a temperature chamber (Jeiotech TH-G-408) and a main PC. The current and terminal voltage of the cell were measured accurately by the Maccor 4300 K converter with a full-scale range (FSR) measurement error below 0.02%. This experiment was implemented with a controlled temperature of 25 °C.

In this paper, all of the charge-discharge experiments were conducted by: (1) charging the battery with CC-CV mode until the battery reaches the charge cutoff voltage of 4.2 V; (2) discharging the battery with CC mode until the SOC reaches the intended initial SOC, where the SOC is calculated by the Coulomb counting method with a precise current sensor; and (3) conducting the target current cycle. As an example, the sequential current and resulting terminal voltage for the UDDS current profile are shown in Figure 4.

To focus on the intended current cycle and target SOC area, the analysis was conducted only for step 3.

Figure 3. Experimental setup: (1) bidirectional DC/DC converter, (2) personal computer (PC) for data acquisition, (3) temperature chamber, and (4) tied battery cells inside the temperature chamber.

Figure 4. Experimental sequence: (**a**) engaging the current and (**b**) the resulting cell terminal voltage.

4.2. Target Battery Specification and Parameters Extraction

The target battery cell is an INR 18650-25R cylindrical Li-ion battery cell comprising GIC and NMC from SAMSUNG SDI. Before extracting the parameters of the given ECM and SOC-OCV relationship, the pre-cycling procedure including 10 fully charge-discharge cycles was conducted in order to the target battery cell can be warmed-up and ready-to-use state. The equivalent parameters for the 1st-order Thevenin ECM are extracted using an offline hybrid pulse power characterization cycle (HPPC) test at a constant temperature of 25 °C. The current profile and voltage profile of HPPC test are shown in Figure 5.

1 C-rate (2.5A) is chosen for charge-discharge current, and by discharging 30 min with 1 C-rate current, and discharge the battery during 30 min at every cycles so that the SOC level is dropped by 5%. In order to measure the OCV at each SOC level, the battery is rested for an hour. According to the voltage and current data, resulting equivalent parameters and SOC-OCV relationship for each SOC level are shown in Figure 6.
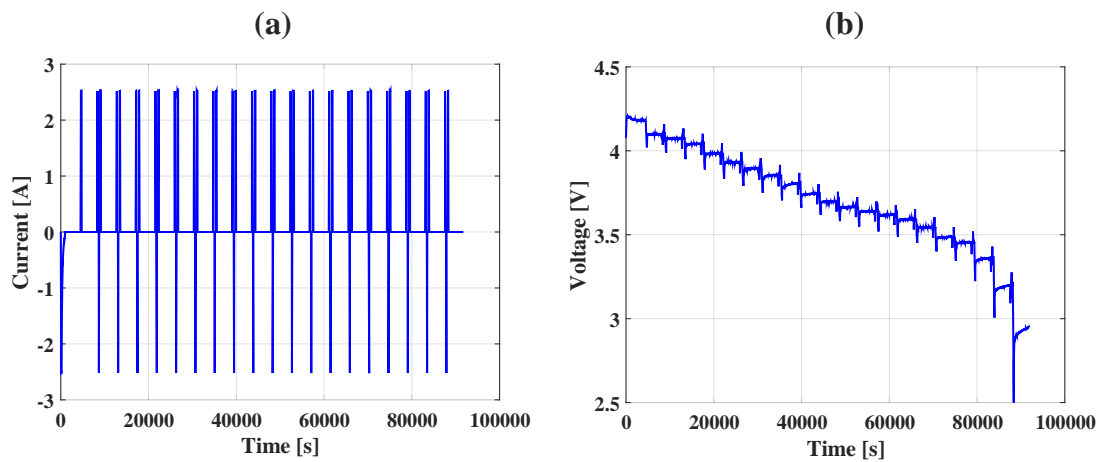
Figure 5. The HPPC test procedure: (**a**) engaged current profile and (**b**) resulting terminal voltage.
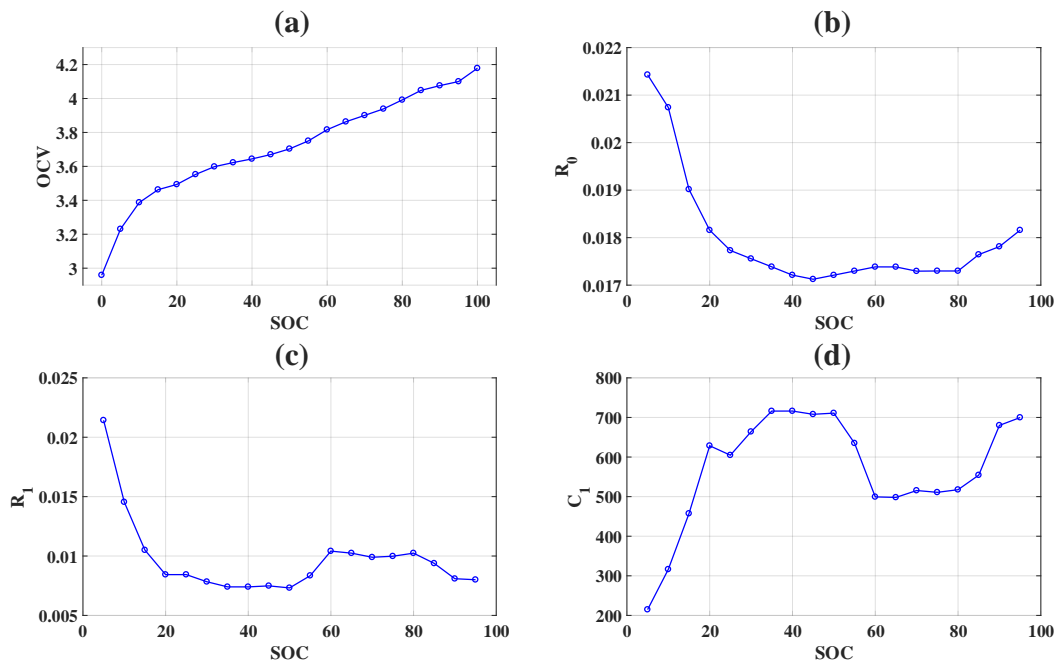

Figure 6. Resulting equivalent parameters: (**a**) SOC-OCV relationship, (**b**) internal resistance (**c**) resistance value of RC-pair and (**d**) capacitance value of RC-pair.

The equivalent parameters are obtained based on the method presented by Kim et al. [44]. The average parameters are listed in Table 1, and these values are used for establishing the state space model and selecting optimal gain of observer.

Table 1. Average values of equivalent parameters of the 1st-order Thevenin ECM.

Parameter	Value
R_0	0.0172 Ω
R_1	0.0097 Ω
C_1	570.86 F
C_n	8972 As

$V_{OC}(z)$ was captured at 5% SOC intervals from 5% SOC to 95% SOC. The linear and nonlinear functions of the proposed OCV representation, which are introduced in Figure 2, are shown in Figure 7.
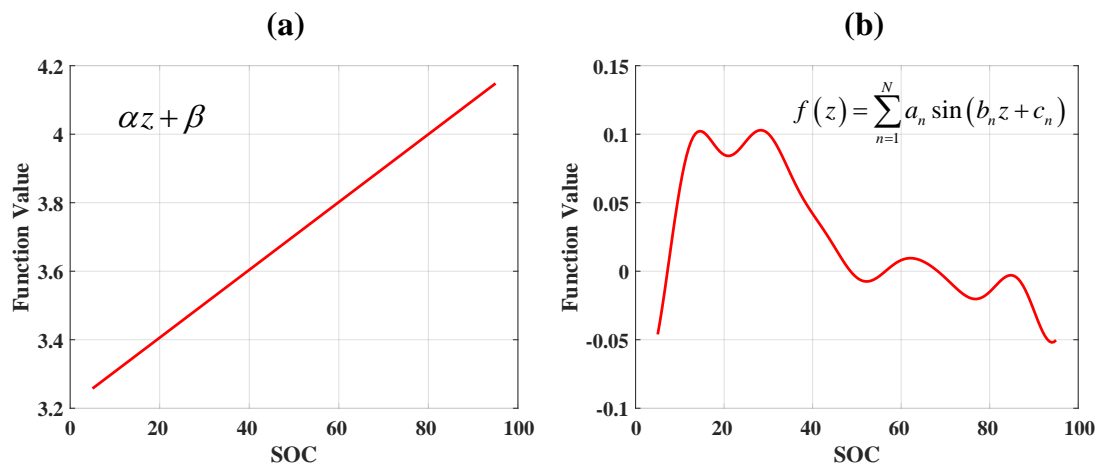
(a) **(b)**

Figure 7. The proposed open-circuit voltage representation: the (**a**) linear term and (**b**) nonlinear term.

The nonlinear term of the OCV function is tuned by utilizing the curve fitting tool in MATLAB (2017a academic version, Mathworks, Natick, MA, USA). The corresponding coefficients are listed in Table 2.

Table 2. Coefficients of the proposed $V_{OC}(z)$ in (6).

Parameter	Value					
α	0.9878					
β	3.2095					
Parameter	**n = 1**	**2**	**3**	**4**	**5**	**6**
a_n	0.07	0.05	0.04	0.02	0.23	0.22
b_n	1.90	0.30	3.39	8.35	10.01	10.10
c_n	−3.30	0.49	−0.98	−1.27	1.74	−1.42

The measured OCV of each 5% SOC and the proposed nonlinear representation of the OCV curve in (6) are shown in Figure 8.
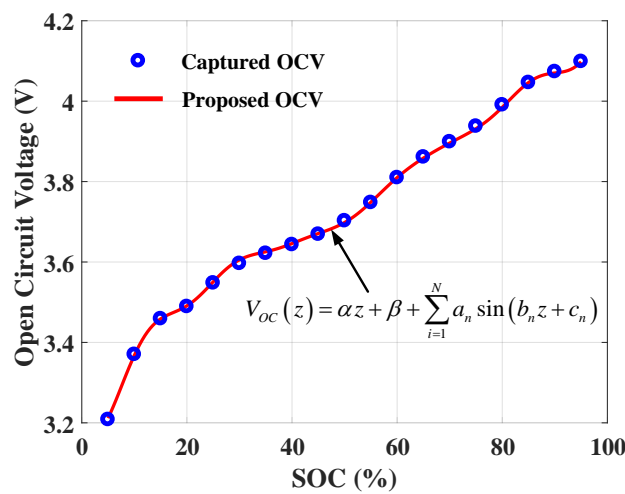

Figure 8. Captured OCV at each SOC point and the SOC-OCV curves fitted using the proposed OCV representation.

Accordingly, the corresponding matrices of the proposed nonlinear battery cell model in (10) are obtained as

$$A = \begin{bmatrix} 0.1018 & 0.2814 & -0.1006 \\ 0 & -0.1796 & 0 \\ 0.0065 & 0.0065 & -0.0064 \end{bmatrix}, \quad C = \begin{bmatrix} 1 & 0 & 0 \end{bmatrix}. \tag{33}$$

From the resulting coefficients, $\alpha = 0.9878$, $p_1 = 0.1018$, $p_2 = 0.1806$, $p_3 = 0.0065$ and the condition in (29), it is known that the linear observability matrix of the given system has full rank. The values of (32) in the overall feasible range of z are shown in Figure 9.
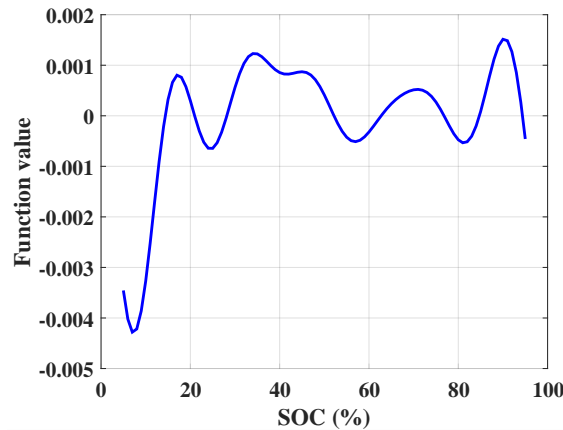
Figure 9. Values of the partial derivative function in (32) for the state in the overall feasible range.

The resulting values are bounded from -0.005 to $+0.002$. This means that the Lipschitz condition in (11) is satisfied if the Lipschitz constant is selected as $\chi > 0.005$. All the necessary conditions of (1) linear observability and the (2) local Lipschitz condition are satisfied. The Luenberger observer gain is selected by utilizing the pole-placement technique so that the eigenvalues of the Luenberger observer satisfy $\lambda(A - L_nC) = \begin{bmatrix} -0.5 & -0.1 & -0.01 \end{bmatrix}^T$ and the sufficient condition in (13) is satisfied. The minimum singular value of $L_n \min_{\omega \in R^+} (A - L_nC - j\omega I)$ is 0.0073. This value is larger than the Lipschitz constant $\chi = 0.005$. From the sufficient condition in (13) of Theorem 1, the proposed observer in (12) with the selected observer gain is asymptotically stable and the state estimation error converges to zero as time increases.

4.3. Experimental Results

The UDDS current profile, which is shown in Figure 4, was used for the experiments. To evaluate the performance of the real-time SOC estimation and insensitivity to sensor noise, two types of experiments were conducted. The first working condition is the noiseless condition. Because the experimental setup has a high precise current and the voltage sensors are operated under controlled conditions, it can be assumed that there is no external noise. There are only unknown model uncertainties. To compare the performance of the SOC estimation of the proposed method with that of previous methods, two types of SOC estimation methods are used: (1) a Luenberger observer with a nonlinear model and (2) an extended Kalman filter (EKF) with following form [45]:

$$\begin{aligned}
x_{k+1} &= Ax_k + Bu_k + \omega_k, \\
y_{k+1} &= C_k x_{k+1} + Du_{k+1} + v_k, \\
A &= \begin{bmatrix} \exp\left(-\frac{\Delta T}{R_1 C_1}\right) & 0 \\ 0 & 1 \end{bmatrix}, \quad B = \begin{bmatrix} R_1\left(1 - \exp\left(-\frac{\Delta T}{R_1 C_1}\right)\right) \\ \frac{\Delta T}{C_n} \end{bmatrix}, \\
C_k &= \left.\frac{\partial V_t}{\partial x}\right|_{x=\hat{x}_{k-1}^-} = \begin{bmatrix} -1 & \frac{\partial V_{OC}(z)}{\partial z} \end{bmatrix}\Big|_{z=\hat{z}_{k-1}^-}, \quad D = [R_0]
\end{aligned} \tag{34}$$

where $x_k = \begin{bmatrix} V_{1,k} & z_k \end{bmatrix}^T$, $y_k = V_{t,k}$, $u_k = I_{L,k}$ and ΔT is the sampling time.

4.3.1. Case 1: Noiseless Condition

The real-time SOC estimation results of the two methods under noiseless condition are shown in Figure 10. The percentage error is calculated by

$$Percent\ error\ (\%) = \frac{True\ value - Estimated\ value}{True\ value} \times 100. \tag{35}$$

At the beginning of the experiment, the initial SOC value is set to be far from the true SOC value. This shows the observer's robustness to the initial state error. As shown in Figure 10, both SOC estimation methods have good performance. Because the EKF is an adaptive and optimal version of the Luenberger observer, it usually shows better performance when the accuracy of the model is sufficiently high and the external noise can be assumed to be Gaussian noise. The EKF also shows a shorter offset compensation time for a well-conditioned experiment than the proposed method. However, after the offset compensation time, the percentage errors of the SOC estimation of the proposed method and the EKF are under ±5%.
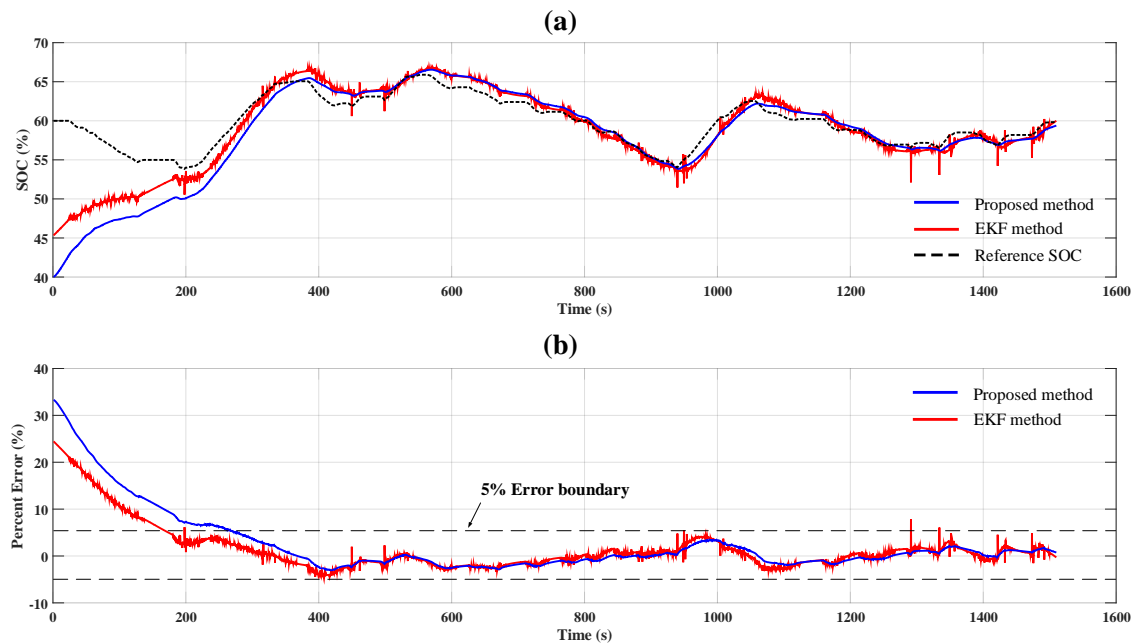
Figure 10. SOC estimation results under noiseless conditions: (**a**) SOC estimation results of the two types of methods and the (**b**) percentage error of each method.

The sensor noise is considered for the other working condition. Two types of sensor noise, voltage sensor noise n_V and current sensor noise n_I, are considered as random noise with zero mean and different peak-to-peak values of $|n_V|_{max} = 0.02\,\text{V}$ and $|n_I|_{max} = 2.5\,\text{A}$. Although the given voltage and current sensor noise conditions are quite severe, this level of sensor noise can occur in a real implementation of an onboard BMS as a result of external noise due to an unstable ground, electromagnetic interference (EMI) from electronic equipment or a low sensor resolution, and as a result, the advanced performance of the proposed method can be emphasized. The current and voltage signals with sensor noise are shown in Figure 11.

(a)

(b)
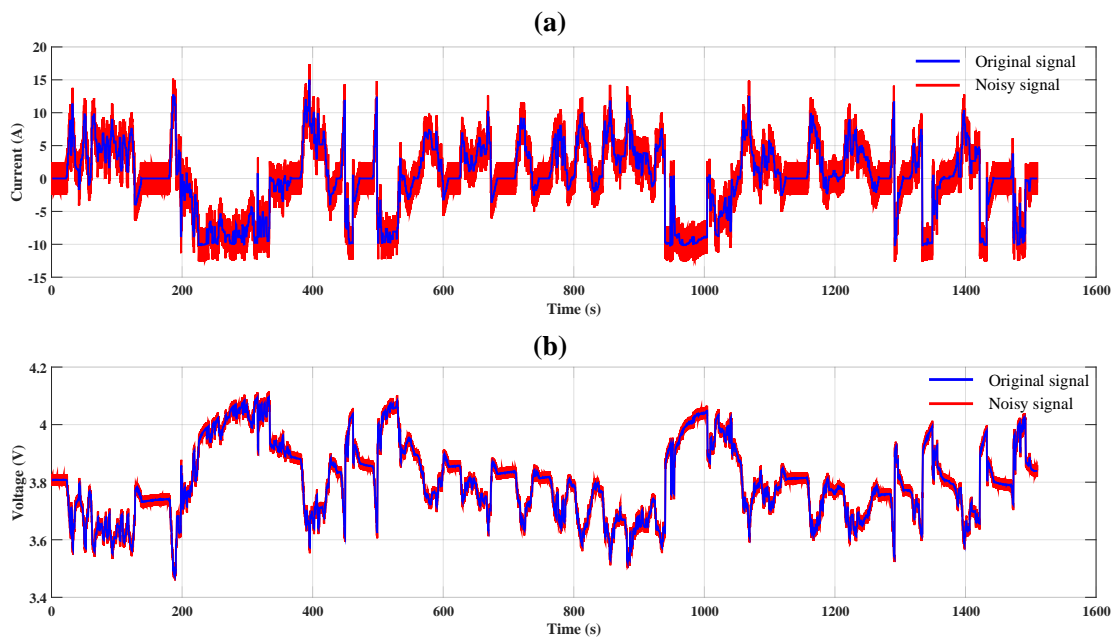
Figure 11. Voltage and current signals: (**a**) original and noisy current signal and (**b**) original and noisy voltage signal.

4.3.2. Case 2: Voltage Sensor Noise Condition

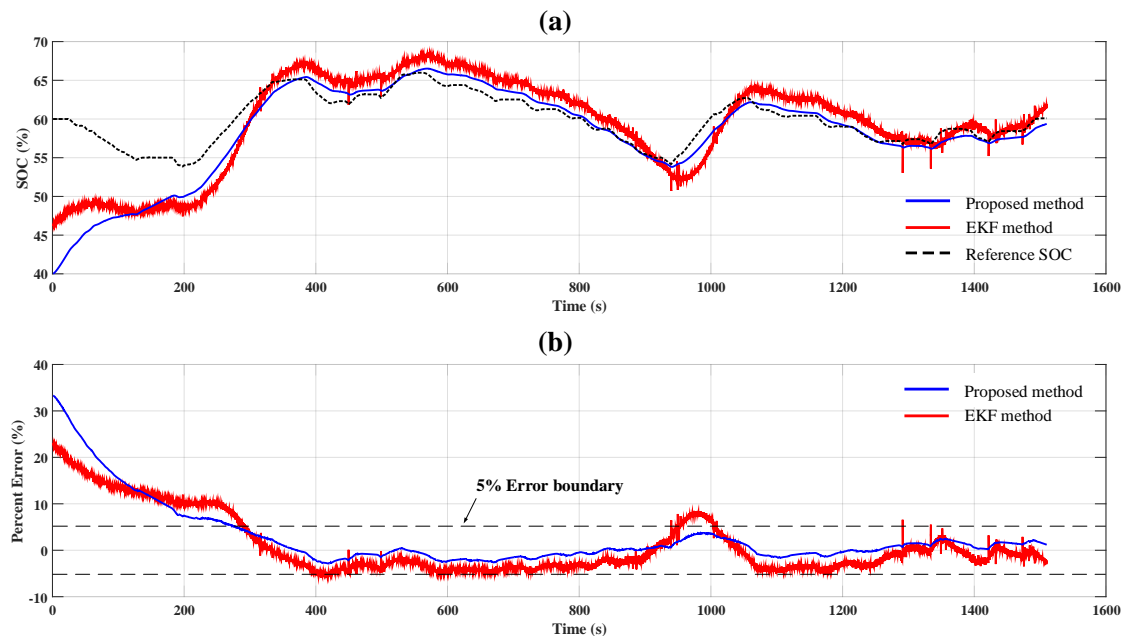Figure 12 shows the SOC estimation results with only voltage sensor noise.

(a)

(b)
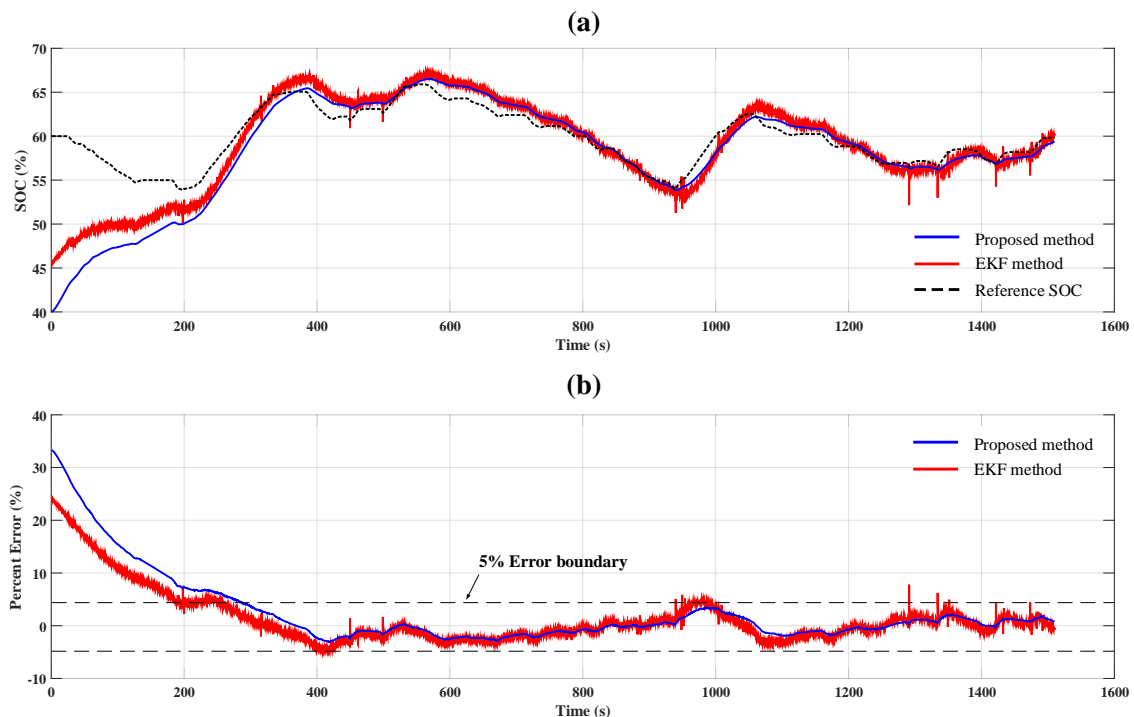
Figure 12. SOC estimation results with voltage sensor noise: (**a**) SOC estimation results of the two types of methods and (**b**) percentage error of each method.

As shown in (34), the output vector y is the measured terminal voltage. Because the EKF is a good estimator whether the measurement noise can be assumed Gaussian noise, EKF shows better SOC estimation performance compared with proposed method by suppressing the voltage noise well.

The percentage error and offset compensating time are slightly increased compared with the results of the noiseless condition.

4.3.3. Case 3: Voltage and Current Sensor Noise Condition

Figure 13 shows the SOC estimation results with voltage and current sensor noise.

Figure 13. SOC estimation results with voltage and current sensor noise: (**a**) SOC estimation results of the two types of methods and (**b**) percentage error of each method.

Table 3 summarizes the results of the two types of experiments using both methods. Compared with the results of the noiseless experiment, the SOC estimation error is larger with both methods because of the sensor noise. However, in the case of the proposed method, the increases in the mean absolute error (MAE) and the maximum error (after the offset compensation) are relatively smaller than those of the errors of the EKF. The time for compensating the initial offset (when the percentage error is less than 5%) is less affected by the sensor noise.

Table 3. SOC estimation results for different experimental conditions using both methods.

Method	Experiment	Offset Compensation Time (s)	MAE (%)	Absolute Maximum Error (%)
Extended Kalman filter	Noiseless condition	174.59	2.9099	4.1340
	Noise condition	294.62	4.8255	7.8403
Proposed method	Noiseless condition	274.36	3.7413	3.3539
	Noise condition	278.96	3.7646	3.6544

This result occurs because the proposed method includes the terminal voltage in the state vector. Although the terminal voltage of the battery is information that can be measured, the result of adding this information to the state vector is that it is updated when integrating the error between the noisy measurement signal and the estimated value. The block diagram of proposed method is shown in Figure 14.

It is shown that at the last sequence, the state vector is passed through the integrator. This integrator can suppress the zero mean noisy signal in the state vector, which it is similar to the low-pass filter. As a disadvantage, this can decrease the state estimation response. Therefore, it is necessary to set an appropriate gain and achieve a trade-off between these characteristics. On the other hand, the EKF directly updates the state values by using the noisy measurement signal. According to

the given model in (34), different from the voltage sensor noise, the current sensor noise is applied to not only the output vector through the matrix D but also the state vector through the matrix B. It means that if there exists current sensor noise, both the measured value $y(k)$ and the estimated states $x(k)$ based on the system model are inaccurate. Therefore, Kalman filter cannot show the convincing performance under this kinds of condition because Kalman filter is designed to estimate the state with a more accurate value between the measured value and the estimated value. This condition occurs neither of these values is accurate. Figure 15 shows the estimated voltage of both the proposed method and the original voltage signal.

It is known that in the case of the EKF, the noisy voltage signal is directly used for updating the SOC, but in the case of the proposed method, although the estimation speed is relatively slow, the noisy signal is filtered out.
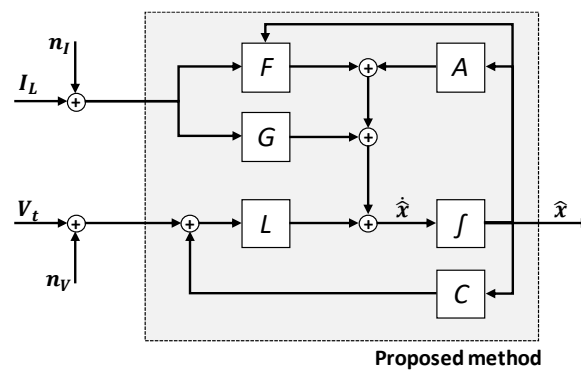

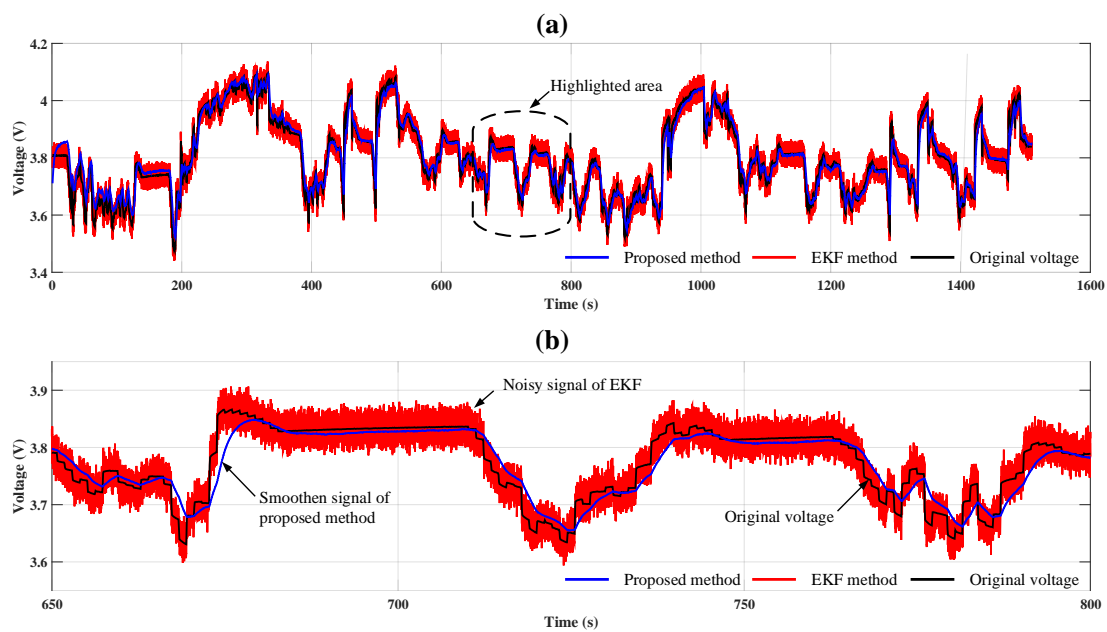
Figure 14. The block diagram of proposed method.

Figure 15. (**a**,**b**) Estimated voltage of both methods and the original voltage signal.

Therefore, the proposed method can robustly estimate the SOC in the presence of sensor noise.

5. Discussion

Although not experimentally verified in this paper, the proposed nonlinear battery cell model can solve the critical limitation of the linearized model in (5). The observability matrix of a given linearized model is calculated as

$$O\left(A,C\right) = \begin{bmatrix} C & CA \end{bmatrix}^{T} = \begin{bmatrix} -1 & k_i \\ \frac{1}{C_1 R_1} & 0 \end{bmatrix}. \tag{36}$$

By calculating the determinant of the observability matrix, the observability condition of the linear system is obtained as

$$\det\left|O\left(A,C\right)\right| = -k_i \frac{1}{C_1 R_1}. \tag{37}$$

The condition directly states that the given linearized system is observable only if $k_i \neq 0$. That is, if there is a flat voltage region in the open-circuit voltage curve, the linearized model loses its observability. This situation can occur in certain battery types: e.g., LiFePO$_4$ (LFP). The LFP-type battery has voltage plateaus in the SOC-OCV curve [36–38,46]. Therefore, when the SOC range is within such an area, the linearized model cannot estimate the SOC from the OCV curve because there is no state excitation. Previous studies did not consider such problems.

Simulation Study with a Virtual Battery Cell Having Wide Range of Flat OCV Curve

Let assume that there exist a virtual battery cell having flat OCV curve from 20 % to 80 % SOC range. The SOC-OCV relationship of this battery cell is shown in Figure 16, and two kinds of model (1) proposed OCV curve representation in (2) and (2) linearized OCV curve representation in (4) are used for SOC-OCV curve fitting.
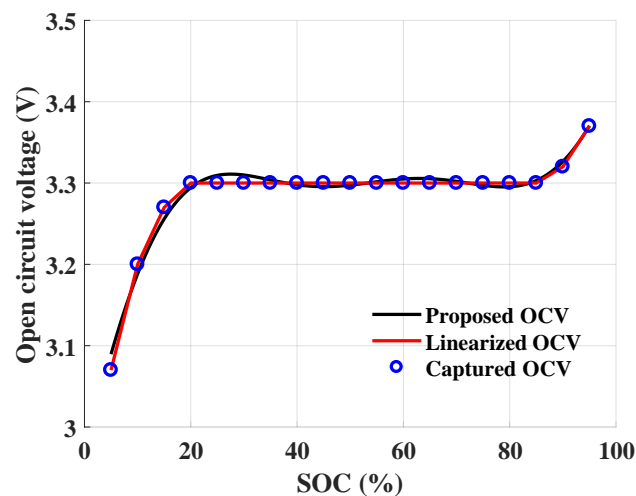
Figure 16. SOC-OCV relationship with wide flat area and two kinds of representation of OCV curve.

The SOC estimation results of proposed nonlinear-model in (10) and linearized model in (5) are shown in Figure 17.

As derived in (37), the linearized model loses its observability when there exists flat area on the OCV curve. Thus, the estimated SOC cannot converge to the true value. However, the observability condition of the proposed nonlinear-model is independent of the form of the OCV curve. It is shown that the estimated SOC based on the nonlinear-model converges to the true value. This result has been obtained empirically, and mathematical validation remains as a further research.
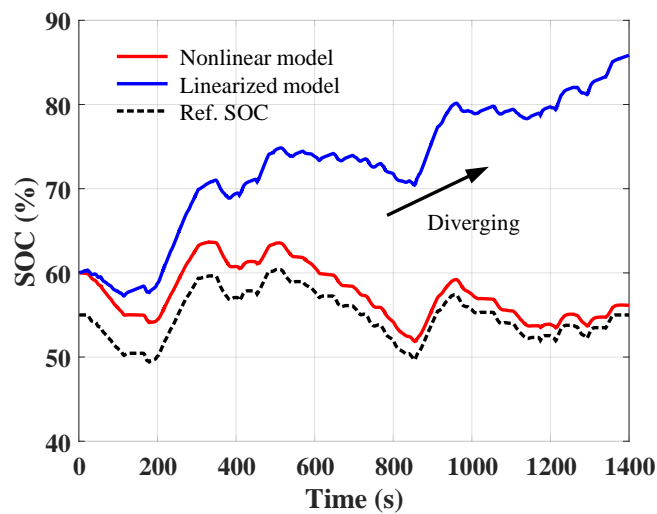
Figure 17. SOC estimation result with nonlinear model and linearized model.

6. Conclusions

This study has proposed a nonlinear state space representation for a Li-ion battery cell and Luenberger observer for a class of nonlinear systems. The proposed nonlinear battery cell model contains the terminal voltage in the state vector, improving the robustness against sensor noise caused by the external operating environment or sensor faults. The proposed method has improved SOC estimation performance in the presence of sensor noise. The improvements of the proposed nonlinear-model-based method are demonstrated with experiments; however, there is room for improvement in this study. Because the proposed observer is a Luenberger observer, an additional performance enhancement can be achieved by adding adaptive observe gain, such as sliding-mode gain and integral gain. However, verifying the stability condition of these observers for nonlinear systems is much more challenging. Thus, this will be considered in a future study.

Conflicts of Interest: The authors declare no conflict of interest.

Abbreviations

The following abbreviations are used in this manuscript:

HEV	Hybrid electric vehicle
EV	Electric vehicle
BMS	Battery management system
Li-ion	Lithium-ion
SOC	State of charge
ANN	Artificial neural network
EECM	Equivalent Electrochemical model
ECM	Equivalent circuit model
OCV	Open-circuit voltage
HPPC	Hybrid pulse power characterization
UDDS	Urban dynamometer driving schedule
MAE	Mean absolute error
LFP	LiFePO$_4$; Lithium-ion phosphate battery
EKF	Extended Kalman filter

References

1. Zhou, L.; Zheng, Y.; Ouyang, M.; Lu, L. A study on parameter variation effects on battery packs for electric vehicles. *J. Power Sources* **2017**, *364*, 242–252. [CrossRef]
2. He, H.; Qin, H.; Sun, X.; Shui, Y. Comparison Study on the Battery SoC Estimation with EKF and UKF Algorithms. *Energies* **2013**, *6*, 5088–5100. [CrossRef]
3. Rezvanizaniani, S.M.; Liu, Z.; Chen, Y.; Lee, J. Review and recent advances in battery health monitoring and prognostics technologies for electric vehicle (EV) safety and mobility. *J. Power Sources* **2014**, *256*, 110–124. [CrossRef]
4. Lu, L.; Han, X.; Li, J.; Hua, J.; Ouyang, M. A review on the key issues for lithium-ion battery management in electric vehicles. *J. Power Sources* **2013**, *226*, 272–288. [CrossRef]
5. Hannan, M.A.; Lipu, M.S.H.; Hussain, A.; Mohamed, A. A review of lithium-ion battery state of charge estimation and management system in electric vehicle applications: Challenges and recommendations. *Renew. Sustain. Energy Rev.* **2017**, *78*, 834–854. [CrossRef]
6. Ali, M.U.; Zafar, A.; Nengroo, S.H.; Hussain, S.; Alvi, M.J.; Kim, H.J. Towards a Smarter Battery Management System for Electric Vehicle Applications: A Critical Review of Lithium-Ion Battery State of Charge Estimation. *Energies* **2019**, *12*, 446. [CrossRef]
7. Hoque, M.M.; Hannan, M.A.; Mohamed, A.; Ayob, A. Battery charge equalization controller in electric vehicle applications: A review. *Renew. Sustain. Energy Rev.* **2017**, *75*, 1363–1385. [CrossRef]
8. Nitta, N.; Wu, F.; Lee, J.T.; Yushin, G. Li-ion battery materials: Present and future. *Mater. Today* **2015**, *18*, 252–264. [CrossRef]
9. He, W.; Williard, N.; Chen, C.; Pecht, M. State of charge estimation for electric vehicle batteries using unscented kalman filtering. *Microelectron. Reliab.* **2013**, *53*, 840–847. [CrossRef]
10. Xia, B.; Wang, H.; Tian, Y.; Wang, M.; Sun, W.; Xu, Z. State of Charge Estimation of Lithium-Ion Batteries Using an Adaptive Cubature Kalman Filter. *Energies* **2015**, *8*, 5916–5936. [CrossRef]
11. Fang, Q.; Wei, X.; Dai, H. A Remaining Discharge Energy Prediction Method for Lithium-Ion Battery Pack Considering SOC and Parameter Inconsistency. *Energies* **2019**, *12*, 987. [CrossRef]
12. Yang, N.; Zhang, X.; Li, G. State of charge estimation for pulse discharge of a LiFePO4 battery by a revised Ah counting. *Electrochim. Acta* **2015**, *151*, 63–71. [CrossRef]
13. Ng, K.S.; Moo, C.S.; Chen, Y.P.; Hsieh, Y.C. Enhanced coulomb counting method for estimating state-of-charge and state-of-health of lithium-ion batteries. *Appl. Energy* **2009**, *86*, 1506–1511. [CrossRef]
14. Weigert, T.; Tian, Q.; Lian, K. State-of-charge prediction of batteries and battery–supercapacitor hybrids using artificial neural networks. *J. Power Sources* **2011**, *196*, 4061–4066. [CrossRef]
15. Shen, Y. Adaptive online state-of-charge determination based on neuro-controller and neural network. *Energy Convers. Manag.* **2010**, *51*, 1093–1098. [CrossRef]

16. Lai, X.; Qiao, D.; Zheng, Y.; Zhou, L. A Fuzzy State-of-Charge Estimation Algorithm Combining Ampere-Hour and an Extended Kalman Filter for Li-Ion Batteries Based on Multi-Model Global Identification. *Appl. Sci.* **2018**, *8*, 2028. [CrossRef]

17. Plett, G.L. *Battery Management Systems, Volume I: Battery Modeling*; Artech House: Norwood, MA, USA, 2015.

18. Nikolian, A.; Hoog, J.D.; Fleurbay, K.; Timmermans, J.M.; Noshin, O.; Bossche, P.V.D.; Mierlo, J.V. Classification of Electric modelling and Characterization methods of Lithium-ion Batteries for Vehicle Applications. In Proceedings of the European Electric Vehicle Congress, Brussels, Belgium, 2–5 December 2014; pp. 1–15.

19. Nikolian, A.; Firouz, Y.; Gopalakrishnan, R.; Timmermans, J.M.; Omar, N.; van den Bossche, P.; van Mierlo, J. Lithium Ion Batteries—Development of Advanced Electrical Equivalent Circuit Models for Nickel Manganese Cobalt Lithium-Ion. *Energies* **2016**, *9*, 360. [CrossRef]

20. Lee, S.; Kim, J.; Lee, J.; Cho, B.H. State-of-charge and capacity estimation of lithium-ion battery using a new open-circuit voltage versus state-of-charge. *J. Power Sources* **2008**, *185*, 1367–1373. [CrossRef]

21. Nejad, S.; Gladwin, D.T.; Stone, D.A. A systematic review of lumped-parameter equivalent circuit models for real-time estimation of lithium-ion battery states. *J. Power Sources* **2016**, *316*, 183–196. [CrossRef]

22. He, H.; Xiong, R.; Fan, J. Evaluation of Lithium-Ion Battery Equivalent Circuit Models for State of Charge Estimation by an Experimental Approach. *Energies* **2011**, *4*, 582–598. [CrossRef]

23. Sun, Q.; Zhang, H.; Zhang, J.; Ma, W. Adaptive Unscented Kalman Filter with Correntropy Loss for Robust State of Charge Estimation of Lithium-Ion Battery. *Energies* **2018**, *11*, 3123. [CrossRef]

24. Jung, S.; Jeong, H. Extended Kalman Filter-Based State of Charge and State of Power Estimation Algorithm for Unmanned Aerial Vehicle Li-Po Battery Packs. *Energies* **2017**, *10*, 1237. [CrossRef]

25. Diab, Y.; Auger, F.; Schaeffer, E.; Wahbeh, M. Estimating Lithium-Ion Battery State of Charge and Parameters Using a Continuous-Discrete Extended Kalman Filter. *Energies* **2017**, *10*, 1075. [CrossRef]

26. Yu, Z.; Huai, R.; Xiao, L. State-of-Charge Estimation for Lithium-Ion Batteries Using a Kalman Filter Based on Local Linearization. *Energies* **2015**, *8*, 7854–7873. [CrossRef]

27. He, Z.; Gao, M.; Wang, C.; Wang, L.; Liu, Y. Adaptive State of Charge Estimation for Li-Ion Batteries Based on an Unscented Kalman Filter with an Enhanced Battery Model. *Energies* **2013**, *6*, 4134–4151. [CrossRef]

28. Hu, X.; Sun, F.; Zou, Y. Estimation of State of Charge of a Lithium-Ion Battery Pack for Electric Vehicles Using an Adaptive Luenberger Observer. *Energies* **2010**, *3*, 1586–1603. [CrossRef]

29. Tian, Y.; Chen, C.; Xia, B.; Sun, W.; Xu, Z.; Zheng, W. An Adaptive Gain Nonlinear Observer for State of Charge Estimation of Lithium-Ion Batteries in Electric Vehicles. *Energies* **2014**, *7*, 5995–6012. [CrossRef]

30. Kim, I.S. The novel state of charge estimation method for lithium battery using sliding mode observer. *J. Power Sources* **2006**, *163*, 584–590. [CrossRef]

31. Kim, D.; Koo, K.; Jeong, J.; Goh, T.; Kim, S. Second-Order Discrete-Time Sliding Mode Observer for State of Charge Determination Based on a Dynamic Resistance Li-Ion Battery Model. *Energies* **2013**, *6*, 5538–5551. [CrossRef]

32. Chen, X.; Shen, W.; Cao, Z.; Kapoor, A. A novel approach for state of charge estimation based on adaptive switching gain sliding mode observer in electric vehicles. *J. Power Sources* **2014**, *246*, 667–678. [CrossRef]

33. Jun, X.; Mi, C.C.; Binggang, C.; Junjun, D.; Zheng, C.; Siqi, L. The State of Charge Estimation of Lithium-Ion Batteries Based on a Proportional-Integral Observer. *IEEE Trans. Veh. Technol.* **2014**, *63*, 1614–1621. [CrossRef]

34. Tang, X.; Liu, B.; Lv, Z.; Gao, F. Observer based battery SOC estimation: Using multi-gain-switching approach. *Appl. Energy* **2017**, *204*, 1275–1283. [CrossRef]

35. Klee Barillas, J.; Li, J.; Günther, C.; Danzer, M.A. A comparative study and validation of state estimation algorithms for Li-ion batteries in battery management systems. *Appl. Energy* **2015**, *155*, 455–462. [CrossRef]

36. Zheng, Y.; Ouyang, M.; Lu, L.; Li, J.; Han, X.; Xu, L.; Ma, H.; Dollmeyer, T.A.; Freyermuth, V. Cell state-of-charge inconsistency estimation for LiFePO4 battery pack in hybrid electric vehicles using mean-difference model. *Appl. Energy* **2013**, *111*, 571–580. [CrossRef]

37. Zhang, C.; Jiang, J.; Zhang, L.; Liu, S.; Wang, L.; Loh, P. A Generalized SOC-OCV Model for Lithium-Ion Batteries and the SOC Estimation for LNMCO Battery. *Energies* **2016**, *9*, 900. [CrossRef]

38. Wang, L.; Lu, D.; Liu, Q.; Liu, L.; Zhao, X. State of charge estimation for LiFePO4 battery via dual extended kalman filter and charging voltage curve. *Electrochim. Acta* **2019**, *296*, 1009–1017. [CrossRef]

39. Zou, Z.; Xu, J.; Mi, C.; Cao, B.; Chen, Z. Evaluation of Model Based State of Charge Estimation Methods for Lithium-Ion Batteries. *Energies* **2014**, *7*, 5065–5082. [CrossRef]

40. Francis, B.A. *Course in H$_\infty$ Control Theory. Lectures Notes in Control and Information Sciences*; Springer Verlag: Berlin/Heidelberg, Germany, 1987.

41. Rajamani, R. Observers for Lipschitz Nonlinear Systems. *IEEE Trans. Autom. Control* **1998**, *43*, 397–401. [CrossRef]

42. Khalil, H.K.; Grizzle, J.W. *Nonlinear Systems*; Prentice Hall: Upper Saddle River, NJ, USA, 2002; Volume 3.

43. Chen, Z.; Li, X.; Shen, J.; Yan, W.; Xiao, R. A Novel State of Charge Estimation Algorithm for Lithium-Ion Battery Packs of Electric Vehicles. *Energies* **2016**, *9*, 710. [CrossRef]

44. Kim, J.H.; Lee, S.J.; Lee, J.M.; Cho, B.H. A New Direct Current Internal Resistance and State of Charge Relationship for the Li-Ion Battery Pulse Power Estimation. In Proceedings of the 7th International Conference on Power Electronics 2007, Daegu, Korea, 22–26 October 2007.

45. Plett, G.L. *Battery Management Dystems, Volume II: Equivalent-Circuit Methods*; Artech House: Norwood, MA, USA, 2015.

46. Gerschler, J.B.; Sauer, D.U. Investigation of open-circuit-voltage behaviour of lithium-ion batteries with various cathode materials under special consideration of voltage equalisation phenomena. In Proceedings of the EVS24 International Battery, Hybrid and Fuel Cell Electric Vehicle Symposium, Stavanger, Norway, 13–16 May 2009.